DOE/ER/40561-166-INT93-12-03

NUCLEAR EFFECTIVE FORCES AND ISOTOPE SHIFTS

P.G. Reinhard

Institut für Theoretische Physik
Universität Erlangen
Staudstr. 7
D-91058 Erlangen, Germany

H. Flocard

Division de Phys. Théorique
Inst. Phys. Nucléaire
B.P. 1
F-91406 Orsay Cedex, France

PREPARED FOR THE U.S. DEPARTMENT OF ENERGY
UNDER GRANT DE-FG06-90ER40561

This report was prepared as an account of work sponsored by the United States Government. Neither the United States nor any agency thereof, nor any of their employees, makes any warranty, express or implied, or assumes any legal liability or responsibility for the accuracy, completeness, or usefulness of any information, apparatus, product, or process disclosed, or represents that its use would not infringe privately owned rights. Reference herein to any specific commercial product, process, or service by trade name, mark, manufacturer, or otherwise, does not necessarily constitute or imply its endorsement, recommendation, or favoring by the United States Government or any agency thereof. The views and opinions of authors expressed herein do not necessarily state or reflect those of the United States Government or any agency thereof.

MASTER

DISTRIBUTION OF THIS DOCUMENT IS UNLIMITED

DISCLAIMER

Portions of this document may be illegible in electronic image products. Images are produced from the best available original document.

Nuclear effective forces and isotope shifts

P.-G. Reinhard* and H. Flocard†
Institute for Nuclear Theory, Seattle , USA

Abstract

Presently availaible relativistic and nonrelativistic effective interactions do not predict the same behavior for the isotope shifts in the *Pb* region. We analyze this difference and find that it is related to the characteristics of the spin-orbit term used in the parametrizations. We show that a simple modification of the spin-orbit contribution to the nonrelativistic Skyrme functional solves this problem.

1 Introduction

Since more than two decades, nuclear mean-field models using effective energy functionals have been a succesful tool to microscopically describe global properties of the nuclear ground states, collective motion, and giant resonances. Among the nonrelativistic models, the most widely used is probably the Skyrme Hartree-Fock (SHF) model for which first well balanced parametrizations appeared in [1] (for an early review see [2]). There exists now a relativistic analogue, the relativistic mean-field (RMF) model, which was initiated at the same time [3] but only achieved the same level of quantitative success during the last decade (for reviews see [4, 5]). Both models can be said to be equally succesful at describing bulk nuclear ground state properties, such as energy, radii and surface, as well as deformation properties and fission, see e.g. [5, 6]. In that respect, from a phenomenological point of view, they are very similar. However, differences appear for more detailed observables. For instance, it was pointed out in a recent investigation that the SHF model with standard parametrizations fails

*Institut für Theoretische Physik, Universität Erlangen, Staudtstr. 7, D-91058 Erlangen, Germany
†Permanent addres: Division de Phys. Théorique, Inst. Phys. Nucléaire, B.P. 1, F-91406 Orsay Cedex, France. Laboratoire des universités Paris VI et Paris XI associé au CNRS.

to reproduce the observed charge isotope shifts in *Sr*- and *Pb*-isotopes [7]. Not much later, it was shown that the *Pb* data were well described by the RMF model [8]. From these published results, it would seem that the isotope shifts in the vicinity of major shell closures is an observable for which there exists a qualitative difference in the predictions of the nonrelativistic SHF and the RMF models. We note however, that recently this question has been considered from a completely different point of view in several works [7, 9, 10]. They suggest that another mechanism be invoked to describe the isotope shift (including its odd-even staggering); namely a refined description of the interaction in the pairing channel.

It is the aim of this paper to understand the mechanisms behind the different predictions of the SHF and RMF model for the isotope shifts. We have therefore put aside the interesting question of elaborating a better pairing interaction and have instead focused our attention on the comparison of the structure of the two mean-field models, using the same treatment of pairing correlations in both cases. The comparison is performed in two steps. First, we attempt a clarification of the structural differences between the two models by effecting a formal mapping of the RMF into an effective nonrelativistic Hamiltonian which can be compared with the SHF model. Second, we empirically explore the potentialities of both model by means of least-squares fits to a wide range of ground-state data including data on isotope shifts.

The outline of the paper is the following: In section 2, on the specific case of *Pb* we present and analyze the differences observed for standard parametrizations in the SHF and RMF model and determine the factor responsible for them. In section 3, we do a formal comparison of the effective mean-field Hamiltonians in both models. This leads us to consider a minor generalization of the spin-orbit force in the SHF functional. In section 4, we explore the potentialities of the models by fitting new parametrizations with an emphasis on isotope shifts and compare them with each other.

2 Influence of spin-orbit on the isotope shifts

We first analyze the isotope shift problem using the *Pb* isotope series as a test case. The upper part of fig. 1 presents a comparison of the data on the evolution of the charge square radius for a series of *Pb* isotopes with results of calculations performed with two effective mean field models: the nonrelativistic Skyrme Hartree-Fock (SHF) model, represented here by the SkM* parametrization [11], and the relativistic mean-field model (RMF), represented by the parametrization NL-Z [12] (The NL-Z force which is similar to the widely used NL1 parametrization [13] takes into account the effect

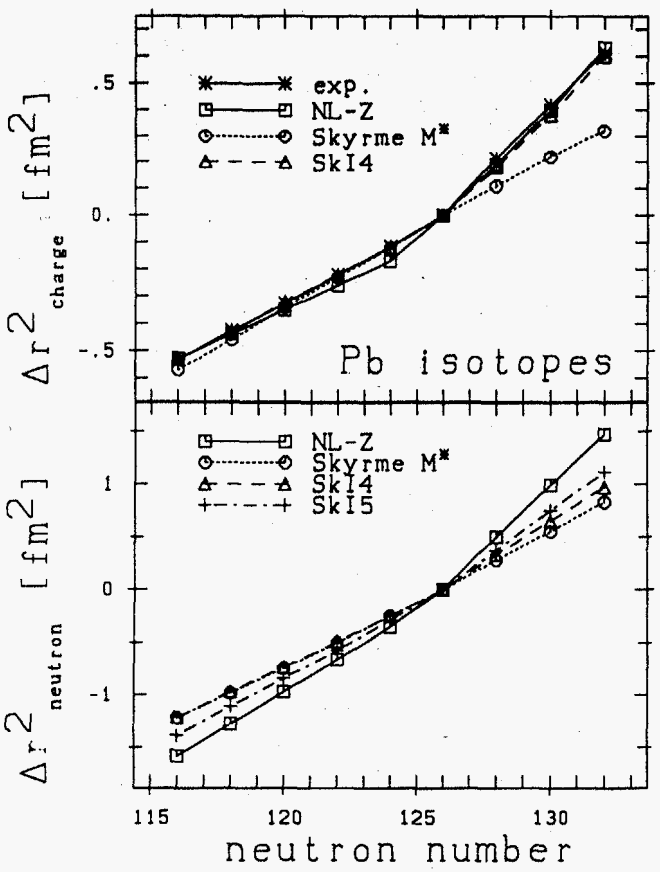

Figure 1:

The squared r.m.s. charge radii (upper part) or neutron radii (lower part) in a chain of even Pb isotopes drawn versus neutron number. The radii are given with respect to ^{208}Pb. We compare the relativistic parametrization NL-Z and several Skyrme forces, the old parametrization "Skyrme M" as well as two new sets SkI4 and SkI5, with the experimental data, as indicated.*

of a more careful treatment of the centre-of-mass correction.). In both calculations a self-consistent BCS treatment of pairing correlations using a constant pairing force of $G_p = 17MeV/A$ for the protons and of $G_n = 23MeV/A$ for the neutrons was effected. The active space was chosen to include the shell above $N = 126$. The magic nuclei ^{208}Pb has been computed without pairing. We have verified that our pairing prescription produces results very close to an alternative using a constant pairing gap $\Delta = 11.2/\sqrt{A}$MeV.

At shell closure, i.e. $N = 126$, the data display a change of the slope which is well reproduced by the RMF model and completely absent from the SkM* results. Looking for the origin of these contrasted results, we have found that the most noticeable difference between the predictions of two models concerns the single particle *neutron* spectrum near the Fermi energy (see upper part of Fig. 2). The difference between the spectra can be traced back to different strengths of the spin-orbit splitting of NL-Z compared to SkM*. For instance, the $1i_{13/2} - 1i_{11/2}$ splitting is 3MeV larger for SkM* than for NL-Z. For the same reason, the energy of the $2g_{9/2}$ orbital is 1MeV lower with SkM*. Since the spatial extension of weakly bound orbitals is strongly related to their single-particle binding energy, one expects the RMF model to give larger radii for the orbitals above the Fermi energy. As can be seen in the lower part of Fig. 2, this is indeed what happens. As a consequence, the progressive filling of the $2g_{9/2}$ orbital in the neutron rich *Pb* isotopes generates a faster growth of the neutron radii for NL-Z than for SkM*.

Pairing correlations also add their contribution to the phenomenon. With SkM*, the $2g_{9/2}$ level is somewhat isolated from the next higher levels reducing therefore the shell gap, see Fig. 2. Moreover the NL-Z single particle level density is high. This leads to a more even spreading of the BCS occupations so that levels with large radii such as the $1i_{11/2}$ contribute more to the neutron density. The Figure 3 shows also that, with NL-Z, some levels close to the continuum (with a large root mean square radius) have a substantial BCS occupation, in contrast with the SkM* case. Note that the modification of the level density found with the SkM* force and the lowering of the $2g_{9/2}$ orbital energy are also due to the larger effective spin-orbit strength. In an analoguous analysis, J.Dobaczewski and W. Nazarewicz [10] also conclude that the spin-orbit strength of SkM* is large.

These three effects explain why the *neutron* radii grow faster for $N > 126$ within the RMF model as can be seen in the lower part of Fig. 1. In fact, the change of slope of the *proton* radius (upper part of the figure) is mostly the attenuated reflection of that which is observed for the neutrons (lower part of the figure). This close connection

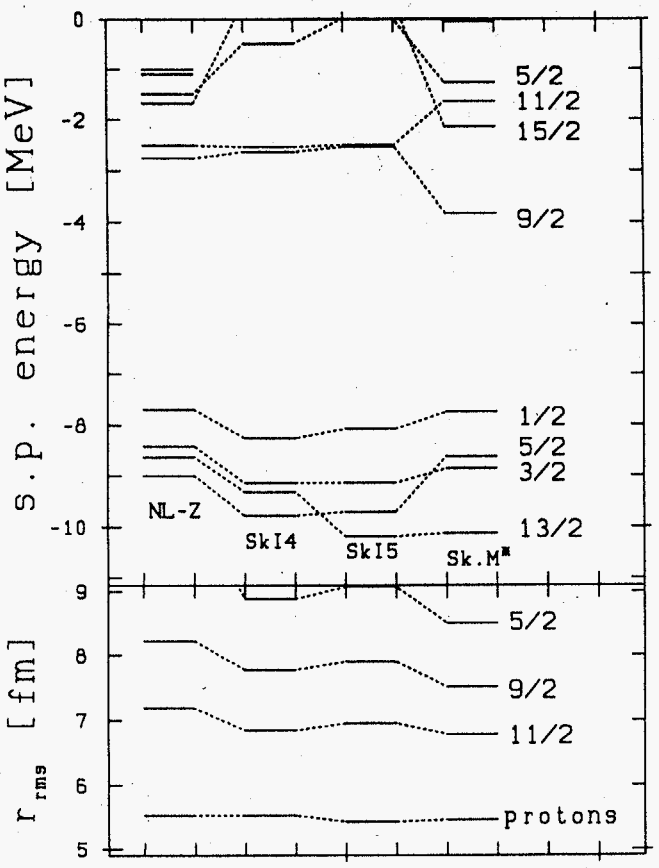

Figure 2:

Upper part: Neutron single particle levels in ^{208}Pb near the Fermi surface for the three parametrizations as indicated. States with equal angular momentum j are connected by a dotted line. The j is given at the right side of the plot. Lower part: Single particle r.m.s. radii for the valence neutron states in ^{208}Pb and, for comparison, the total proton r.m.s. radius as indicated.

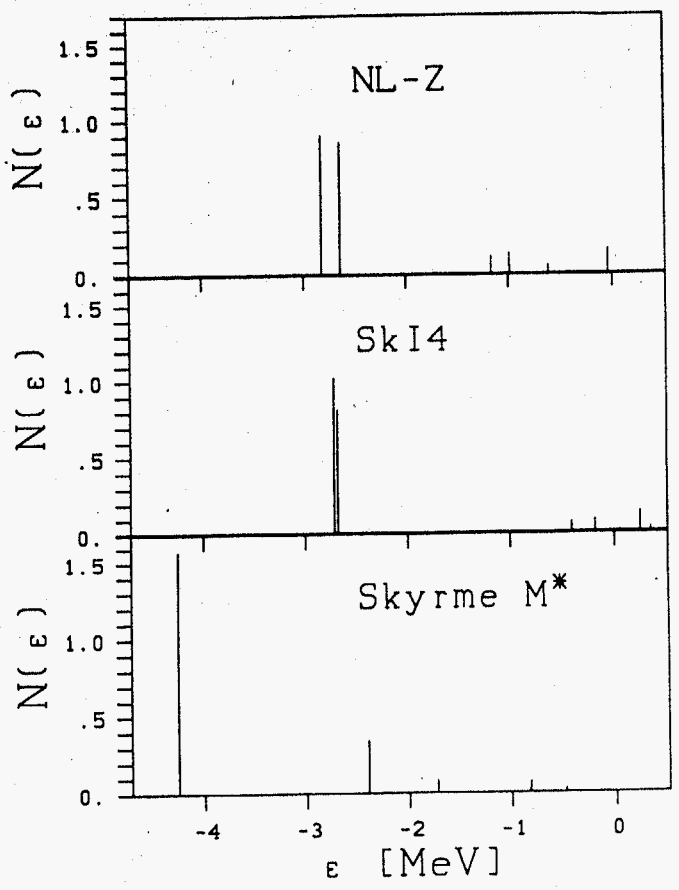

Figure 3:

Distribution of the additional pair of neutrons in ^{210}Pb over the valence states for the three parametrizations as indicated. $N(\varepsilon)$ is the fractional number of neutron in the single particle state with energy ε.

between the neutron and proton spatial distributions results from the self-consistent treatment of the strong p-n attraction in the particle-hole channel.

3 An Extended Skyrme Functional

From the analysis of the previous section we have seen that the origin of the differences between the SkM* and NL-Z results on the evolution of the charge radius of Pb isotopes across the $N = 126$ gap should be traced back to the different neutron single-particle spectra of the two models. As we have further seen that spectra are strongly affected by spin-orbit properties, we now investigate the structure of the spin-orbit terms in the RMF and SHF models.

For a Skyrme-type force the mean-field Hamiltonian for neutrons reads

$$\hat{h} = \hat{p}B\hat{p} + U + W \cdot (\sigma \times \hat{p}) \quad , \tag{1}$$

where the mean-field U, the inverse mass B and the spin-orbit potential W_{ls} are local functionals of the neutron and total densities ρ_n and ρ. The density dependence is linear for the mass and spin-orbit potentials, i.e.

$$B_{SHF} = \frac{\hbar^2}{2m} + b_1\rho + b_1'\rho_n \quad , \tag{2}$$

$$W_{SHF} = b_4(\nabla\rho + \nabla\rho_n) \quad . \tag{3}$$

The expression of the coefficients b_i in terms of the Skyrme force parameters can be found in [14].

One can transform the Dirac equation of the RMF model into an energy -dependent effective Schrödinger equation. This energy-dependence can then be removed via a nonrelativistic expansion which provides an effective Hamiltonian of the form (1), see [5]. The structure of the effective mass and spin-orbit potentials look however different from those derived with the Skyrme force (2). They read

$$B_{RMF} = \frac{\hbar^2}{2m - C_{eff}\rho} \tag{4}$$

$$W_{RMF} = \nabla B = \frac{\hbar^2}{(2m - C_{eff}\rho)^2} C_{eff}\nabla\rho \tag{5}$$

where C_{eff} is related to the scalar and vector coupling strengths ($C_{eff} = g_\sigma^2/m_\sigma^2 + g_\omega^2/m_\omega^2$). In fact, it is not the mass density ρ which enters these expressions, but the density folded with a Yukawa potential whose range is given by the masses of the scalar

and vector mesons. In order to keep the expressions simple we have omitted this feature from the equations (4) and (5). As shown in [5], the solutions of the Schroedinger-like hamiltonian $\hat{h}_{RMF}$ obtained in this way, are very close to those obtained with the original relativistic equation.

Both the Skyrme and RMF-equivalent Hamiltonians have therefore a similar structure with an effective inverse mass B and a spin-orbit potential W. However some differences exist:

1. Folded densities instead of bare densities enter the relativistic expressions of B and W. We have checked that this folding has no significant influence on the nuclear properties discussed in the present article. The test involves a modified Skyrme functional with finite range terms such as those used in the description of liquid ^{3}He [15]. For the nonrelativistic case, we have found that the optimal range is of the order $0.5fm$. We have also checked that a finite range of this order of magnitude has no influence on the isotopic effects discussed hereafter.

2. The way in which neutron and proton densities enter the form factor W is not the same. The effective mass parameter B depends linearly on ρ for a Skyrme force while in the RMF model the same holds for the inverse $1/B$. Moreover the RMF expression for W is weighted by the square of the effective mass parameter. It seems that these different density dependences do not have much importance. We find that SHF and RMF parametrizations producing fits of similar quality on the same large set of nuclear properties lead to B and W functions with comparable radial dependence. This can be seen in Fig. 4 which displays the spin-orbit potentials obtained with SkM* and NL-Z for ^{208}Pb. Both potentials are peaked at the surface and reach their maximum at almost the same radius. The prefactor proportional to B^2 of the RMF model, only causes a small inward shift of the strength which has no detectable physical consequence.

3. The most important difference concerns the spin-orbit strength. On Fig. 4, one sees that the peak of W for the NL-Z force is 30% smaller than for SkM* and the overall strength is even smaller because the peak for NL-Z is much narrower. This strength discrepancy is the major cause for the differences in the neutron spectra discussed in the previous section (Fig. 2).

From these three differences between the RMF and the SHF models, the latter plays the major role in the isotope shift problem. The nonequal spin-orbit strengthes may partly reflect the various strategies adopted in the fitting procedure of SkM* and NL-Z.

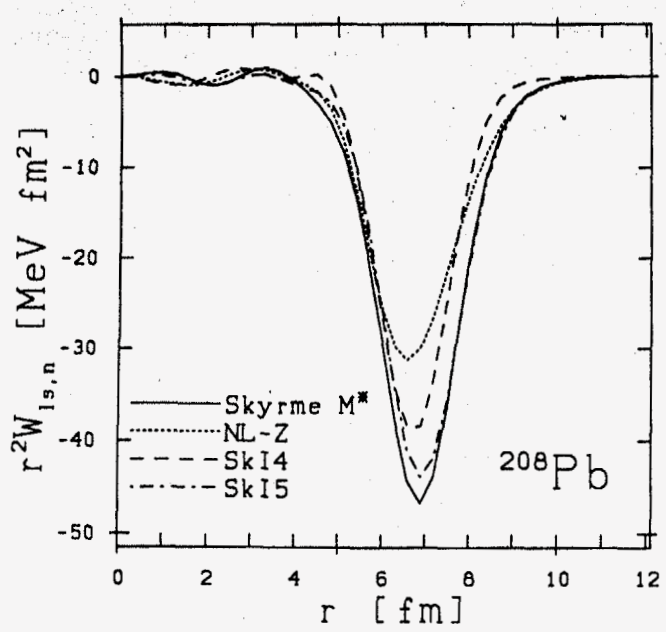

Figure 4:

The neutron spin-orbit potential $W_{ls,n}$ for the four parametrizations as indicated, the relativistic NL-Z, the conventional Skyrme force "Skyrme M", and the two new sets SkI4 and SkI5. The potential is multiplied by the radial weight r^2 to allow a better comparison of the relative strengths.*

On the other hand, they are also certainly related to the structure of the non-relativistic and relativistic W. Whereas W_{SHF} depends on $\rho + \rho_n$, W_{RMF} is only function of the total density ρ only. Thus spin-orbit strengths adjusted on light $N = Z$ nuclei (for instance the $1p$ splitting in ^{16}O) lead to divergent extrapolations for neutron rich heavy nuclei. Because of the additional contribution of ρ_n, the SHF model tends to produce a larger spin-orbit strength in nuclei such as *Pb* isotopes. An earlier investigation of this effect can be found in [16]. As we shall see in Sect. 5, this difference affects also significantly the ability of the functional to reproduce a large body of data.

In order to perform a more detailed investigation of the impact of the spin-orbit force, we consider a simple generalization of the Skyrme functional with a larger flexibility in the isotopic balance within the spin-orbit term. This is achieved by means of an additional coefficient b'_4:

$$\mathcal{E}_{ls} = -\int d^3r \left\{ b_4 \rho \nabla \mathcal{J} + \sum_{q\in\{p,n\}} b'_4 \rho_q \nabla \mathcal{J}_q \right\} \quad . \tag{6}$$

Thus doing, we introduce into the spin-orbit term a degree of freedom which, in fact, is already present in all other components of the Skyrme functional [14]. The definition of the densities $\mathcal{J}$ and $\mathcal{J}_q$ in terms of the orbital wave-functions and their occupation is given in [17, 14]. The spin-orbit potential W for the neutrons becomes

$$W = b_4 \nabla \rho + b'_4 \nabla \rho_n \quad . \tag{7}$$

Therefore, the ratio b'_4/b_4 determines the relative importance of the isovector and isoscalar contributions to the spin-orbit strength. The value of this ratio is unity for the usual Skyrme functional, and zero for the RMF model.

4 Isotopic biased SHF parametrizations

Of the many different available SHF forces we have analyzed, none appears to perform significantly better than SkM* on the *Pb* isotope shift problem. This is not really surprising since this very specific nuclear property has not been considered by the earlier adjustements. On the other hand, it seems to us that one cannot assess the relative virtues of specific models (SHF versus RMF) by discussing their predictions on isotope shift using only the limited set of available parametrizations, which for many of them have not been revisited for more than ten years. In view of the experience accumulated, the improvement in the theoretical methods and the much larger computing power now available, it has become interesting to have a fresh look at the potentialities of the SHF and RMF parametrizations with respect to the additional data brought in by isotope shifts measurements. In any case, the degree of freedom introduced with the functional (6) requires a new adjustment. In the rest of this section, we consider various SHF functionals including the generalized version (6), as well as the RMF model.

4.1 The fitting procedure

We work along the lines already explored in [18, 5]: we perform least-squares fits with respect to nuclear ground state properties for spherical light, medium and heavy nuclei.

	E [MeV]	R_{diff_r} [fm]	σ [fm]
^{16}O	-127.6	2.777	0.839
^{40}Ca	-342.1	3.845	0.978
^{48}Ca	-416.0	3.964	0.881
^{56}Ni	-483.9		
^{58}Ni	-506.5	4.356	
^{84}Sr	-728.9		
^{88}Sr	-768.4	4.994	
^{90}Zr	-783.9	5.040	0.957
^{112}Sn	-953.5	5.477	
^{124}Sn	-1050.0	5.640	
^{132}Sn	-1102.9		
^{146}Gd	-1204.5		
^{208}Pb	-1636.4	6.806	0.900
^{214}Pb	-1663.3		
^{16}O	$\varepsilon_{ls,p}$ = 6.3 MeV		
^{16}O	$\varepsilon_{ls,n}$ = 6.1 MeV		
Pb	$r^2(^{214}Pb)$-$r^2(^{208}Pb)$=0.613 fm^2		
Ca	$r^2(^{48}Ca)$-$r^2(^{40}Ca)$=0.007 fm^2		

Table 1:

Ground state data entering the least-squares fit of the SHF and RMF parameters. Binding energies E, diffraction radii R_{diff_r} and surface thicknesses σ are taken from [19] and [20]. The spin-orbit splitting ε_{ls} between the $1p_{3/2}$ and $1p_{1/2}$ level in ^{16}O is taken as in [1]. The lowest block contains information on the isotope shifts of the two elements Ca and Pb. Radii for the Ca and Pb isotopes come from [21] and [22] respectively.

The observables included in the fits are listed in Table 1. The adopted uncertainty on these data is the same as in our earlier analyses [18, 5]: 0.2% for E, 0.5% for R_{diff_r}, and 1.5% for σ. However, the data set has now been enlarged to include more information on intermediate nuclei and nuclei away from the stability valley. In order to introduce conveniently information on the nuclear charge form factor as measured by electron scattering experiments, we have selected two quantities which determine its gross structure. These are the position of the first zero of the form factor and the height

of the first maximum which can also be related to the diffraction radius R_{diff_r} and the surface thickness parameter σ (for details, see [20]). Many studies comparable to ours use only one observable, the r.m.s. radius, to fix the nuclear shape. We find that at least two quantities are required to adjust correctly volume and surface properties of the nucleon distributions. Note that our charge formfactors are obtained by folding the proton and neutron densities with the electric formfactor of the two species of nucleons. We also take into account the magnetic contributions associated with the spin-orbit currents [23, 24].

As the isotope shift problem provides the motivation for this work we have also included information on the radius evolution versus N for the isotope series of the elements Pb, and Ca. Because data and calculations for Pb always agree for $N \leq 126$ while they can exhibit different behaviors above the magic number (see Fig. 1), we have chosen to investigate the kink at shell closure by considering the quantity

$$\Delta r^2_{charge}(Pb) = r^2_{charge}(^{214}Pb) - r^2_{charge}(^{208}Pb) \quad . \tag{8}$$

In addition, we constrain our parametrization by considering isotope shift data for the medium element Ca. We consider

$$\Delta r^2_{charge}(Ca) = r^2_{charge}(^{48}Ca) - r^2_{charge}(^{40}Ca) \quad . \tag{9}$$

Very early, the charge radii of Calcium isotopes have drawn the attention of nuclear physicists. As N varies from 20 to 28, one does not observe a continuous increase of the radius [25, 26]. The charge radius which begins to grow as one fills the $1f_{7/2}$ shell, diminushes in the second half so that ^{40}Ca and ^{48}Ca have about the same radius.

Another interesting charge radius evolution is that of the Sr isotopes [27]. As an observable typical of this radius sequence we have selected the difference

$$\Delta r^2_{charge}(Sr) = r^2_{charge}(^{84}Sr) - r^2_{charge}(^{88}Sr) = 0.112 fm^2 \quad , \tag{10}$$

for the following reason: as N decreases below $N = 50$ down to $N = 36$, the radius *increases* steadily [27]. The onset of a static prolate deformation predicted by deformed SHF calculations provides a natural explanation for the observed large radii of the isotopes $N \leq 40$. These calculations which find deformation energy surfaces (DES) with deep prolate minima, account well for the radii of these light isotopes [28]. However, when N diminushes from 50 to 46, they predict DES's with spherical minima and a decrease of the radius in contradiction with the data. For N larger than 50, on the other hand, there is again no significant disagreement between data and SHF+BCS results.

The quantity (10) corresponds therefore to one which calculations have difficulties to reproduce.

Another constraint on the force comes from data on excitation properties, such as the giant resonances. The energy of the giant monopole resonance is connected with the incompressibility K of the isospin-symmetric nuclear matter [29]. Studies have shown that within the Skyrme parametrization the magnitude of K is closely related to the power α of the density dependence of the force. On the other hand, due to the uncertainty on the evaluation of finite size and Coulomb contributions to the giant monopole resonance, the value of the incompressibility is probably not known to better than 20%. Assuming that K it is not very different from 240MeV, we have adopted the following power for the density dependence :

$$\alpha = 0.25 \quad . \tag{11}$$

The monopole and nuclear matter properties of the various Skyrme functionals proposed in this work are given in the next subsection. They confirm the validity of the choice (11). In fact, we have also checked that using the values $\alpha = 0.16, 0.20$, and 0.30 did not modify significantly our conclusions concerning fits to ground state properties and isotope shifts.

In order to give more weight to isospin related properties, we have have also added constraints on the giant dipole resonance. Two observables related with this resonance can be exploited: the excitation energy and the dipole sum rule. It turns out that adjustments on ground state data alone leave some freedom concerning the predictions of the Skyrme functional for both resonance observables. As a consequence, one can determine a family of parametrizations of equal quality with respect to ground state properties but with very different dipole resonance energies and sum rules. To remove this indetermination, we have constrained the isovector degrees of freedom of the Skyrme parametrization by fixing the dipole sum rule enhancement factor to

$$\kappa = 0.25 \quad . \tag{12}$$

This quantity κ which measures the deviation with respect to the simple Thomas-Reiche-Kuhn value is only approximately known from experimental data because of the uncertainty on the cutoff energy introduced in the evaluation of the sum rule [30]. On the other hand, recent fits of Skyrme forces covering properties of both known nuclei and neutron matter, see [31], give a strong support to the value (12).

As both the SHF and the RMF models are mean-field descriptions of nuclei, one should consider whether ground-state correlations (GSC) do not prevent a direct comparison of their predictions with data. One source of GSC comes from small amplitude

collective vibrations as described for instance by the RPA. There exists a risk of double counting because effective SHF or RMF models may already incorporate a large fraction of the GSC, more specifically those which behave smoothly versus the mass number A and can therefore be accurately accounted for by the local density approximation (for a detailed example from cluster physics see [32]). We should therefore be mostly concerned with the effect of shell fluctuations on the GSC. Calculations in doubly magic nuclei including all angular momenta up to $L = 7$ show that the effect of RPA correlations on the bulk observables E, R_{diff}, and σ is very small [33]. This justifies the use of the data in Tab. 1 for a direct adjustement of the forces. The quantity by far most sensitive to RPA-GSC is the isotopic difference of r.m.s. radii in Ca which is reduced through RPA-GSC by $-0.69fm^2$ when computed with the force SkM*. In that particular case, the correction is mainly due to the low-lying 3^- state in ^{40}Ca [25, 26]. But the variation of this correction versus N remains small (about $\pm 0.2fm^2$) so that $0.7fm^2$ is a typical order of magnitude for the isotope shift. In the region of Sr and Pb, RPA-GSC are small and can safely be neglected.

Another source of GSC is the coupling to low-lying quadrupole (i.e. 2^+) collective surface vibrations which can be important in non-magic nuclei which are soft against quadrupole deformations. The evaluation of these GSC is a difficult task. It requires the computation of the DES for quadrupole deformations and a solution of the collective dynamics (for examples see [34, 35]). These studies have shown that the energy E and the diffraction radius R_{diff} are not much affected even when the DES corresponds to a soft nucleus. This is the case for all nuclei in the list of Tab. 1. However, surface thickness and r.m.s. radii are more sensitive to this type of collective GSC. This is why, in Tab. 1, we have omited σ as a nuclear observable when we thought that this quantity could be strongly affected by GSC associated with soft vibrations. To estimate the effect of GSC on the isotope shifts we want to study, as a first approximation, one can proceed phenomenologically. One uses the data on $B(E2)$'s to determine an effective β_2 deformation plus fluctuation parameter [25]. Then, this β_2 can be used within the standard liquid drop formula to estimate an associated increase of the squared radius [25]:

$$\delta r^2 = r^2 \frac{5}{4\pi} \beta_2^2 \quad . \tag{13}$$

For the relevant nuclei we obtain: $\beta_2(^{208}Pb) = 0.054$, $\beta_2(^{88}Sr) = 0.117$, and $\beta_2(^{84}Sr) = 0.211$, see [36]. Using (13) for ^{208}Pb one evaluates the r.m.s. correction to be $\delta r^2 = 0.0356fm^2$. We could not find any $B(E2)$ for ^{214}Pb. On the other hand, the collective DES of ^{214}Pb is almost as stiff as that of ^{208}Pb (see Fig. 5). Thus

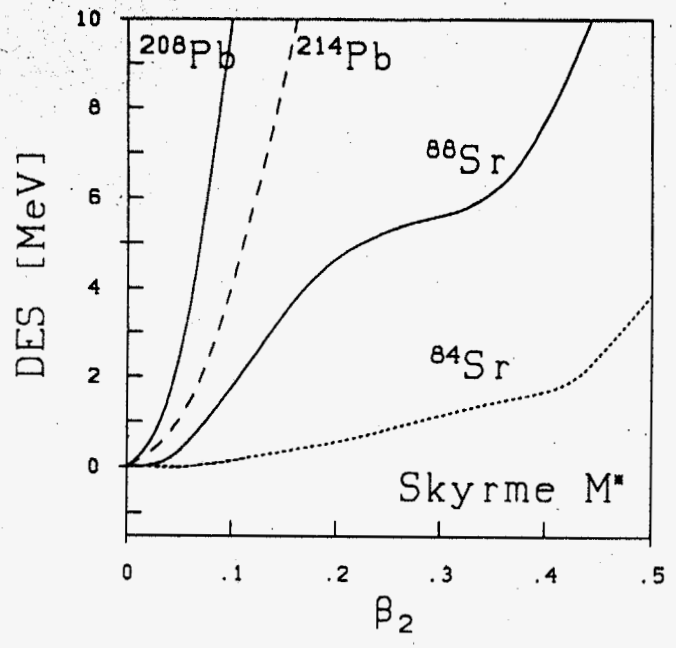

Figure 5:
The deformation energy surfaces (DES) with respect to quadrupole deformation for four nuclei as indicated drawn versus the dimensionless quadrupole moment β_2. All results are computed with the force "Skyrme M".*

we expect the radius correction to be of the same order of magnitude and we take $0.0356 fm^2$ as a measure of the typical uncertainty on the Pb isotope shift (8) from collective GSC. Applying the same method to the isotope shift between ^{84}Sr and ^{88}Sr we find $\delta r^2 = 0.216 fm^2$. This is a very large effect. In fact a microscopic calculation using the generator-coordinate method with SkM* finds only $\delta r^2 = 0.092 fm^2$. On the other hand, the generator-coordinate method seems to underestimate the magnitude of collective vibrations near shell closures. Because of this uncertainty we have excluded the Sr isotope shift from the fitted data set. We nevertheless present the corresponding results obtained with the adjusted functionals. In fact, attempts at fits including a

SkI1	$b'_4 = b_4$	G.S. data	
SkI2	$b'_4 = b_4$	G.S. data	Pb, Ca I.S. data
SkI3	$b'_4 = 0.0$	G.S. data	Pb, Ca I.S. data
SkI4	b'_4 free	G.S. data	Pb, Ca I.S. data
SkI5	$b'_4 = b_4$	G.S. data (no ^{16}O)	Pb, Ca I.S. data

Table 2:
Particulars of the fitting procedure of the five Skyrme-type functionals SkI1-SkI5. In all cases the ground state data (G.S.), and the spin-orbit splitting in ^{16}O given in Tab. 1 have been used. For sets 2 to 5 the data on the isotope shifts (I.S.) of Pb and Ca have been added. To determine SkI5, the ground state of ^{16}O have been omitted from the fitted set.

constraint on Sr isotope shifts have led to forces with unphysical features that we will not discuss here. The low-lying 2^+ state which produces the dominant correlations in non-magic nuclei has only minor effect on the difference between ^{48}Ca and ^{40}Ca. Indeed this state pertains to the harmonic regime and is thus already accounted for in the RPA-GSC.

Using a systematic fitting procedure we have determined five parametrizations of the Skyrme functional which differ either in the way they handle the spin-orbit interaction or in the adjusted data set. The different choices are presented in Tab. 2. The set SkI1 is a refit of the usual Skyrme parametrization with the new data from Tab. 1 and all exchange terms parameters ($x_i, i = 0, \ldots, 3$) included. It can be considered as an updated version of standard Skyrme forces. The set SkI2 which still belongs to the standard Skyrme functional uses the additional information coming from isotope shift data. For the set SkI3, we have imposed the constraint $b'_4 = 0$. In this way, we enforce a density dependence of the spin-orbit formfactor proportional to $\rho = \rho_p + \rho_n$ as in the RMF. With SkI4 we investigate the generalized Skyrme parametrization with the spin-orbit functional (6) as described in Sect. 3.

During the determination of these four functionals, we observed that the optimal fit was most strongly biased by data on ^{16}O. On the other hand, for such a light nucleus one can expect deviations from a pure mean-field picture. For instance one may need an improved treatment of centre-of-mass corrections (see [37]). In order to measure the effect of ^{16}O ground state data on the fitted force, we have also constructed an additional parametrization of a standard Skyrme functional (SkI5) by excluding this

	SkI1	SkI2	SkI3	SkI4	SkI5
t_0	-1913.62	-1915.43	-1762.88	-1855.83	-1772.91
t_1	439.809	438.449	561.608	473.829	550.840
t_2	2697.59	305.446	-227.090	1006.86	-126.685
t_3	10592.3	10548.9	8106.2	9703.61	8206.25
x_0	-0.955	-0.211	0.308	0.405	-0.117
x_1	-5.782	-1.737	-1.172	-2.889	-1.309
x_2	-1.287	-1.534	-1.091	-1.325	-1.049
x_3	-1.561	-0.178	1.293	1.145	0.341
b_4	62.130	60.301	94.254	183.097	61.815
b'_4	62.130	60.301	0.000	-180.351	61.815

Table 3:
Parameters of the Skyrme-type functionals.

particular data from the set of fitted properties.

In Tab. 3, we give the parameters of these five sets with the usual notation [1, 17] except for the spin-orbit parameters for which we use the quantities b_4 and b'_4 defined in Sect. 3.

We have complemented this analysis by a fit of the standard RMF parametrization based on the ground state data and the isotopes shifts in Pb and Ca of Tab. 1. The resulting set is NL-I. As its predictions for the isotope shift in Ca are not satisfactory, we have also investigated a variant of the RMF which takes into account the degrees-of-freedom associated with the tensor couplings of the vector mesons (see e.g. [5]). The corresponding parametrization is refered to as NL-IT.

4.2 Nuclear matter properties

The nuclear matter properties of the functionals Tab. 3 are given in Tab. 4. In this table, the upper block of parametrizations corresponds to functionals optimized without particular emphasis on isotopic trends, whereas the parametrizations in the lower block took care of the extra isotopic data.

The values of the binding energy and equilibrium density, are for all forces close to the commonly accepted values. They do not vary much from one force to the next. The various incompressibilities fall in the range 240 ± 40 which in our opinion measures

	ρ_{nm} [fm^{-3}]	E/A [MeV]	K [MeV]	m^*/m	a_4 [MeV]	$\kappa_{sumrule}$
SkM*	0.161	-16.01	219.2	0.786	30.0	0.54
NL-Z	0.151	-16.19	173.5	0.648	41.8	
NL-SH	0.146	-16.33	355.0	0.662	36.1	
SkI1	0.160	-15.93	242.7	0.693	37.5	0.25
	± 0.001	±0.04	±20.0	± 0.023	± 5.17	
SkI2	0.158	-15.76	240.9	0.685	33.4	0.25
	±0.001	±0.04	±20.0	±0.020	± 1.0	
SkI3	0.158	-15.96	258.1	0.577	34.8	0.25
SkI4	0.160	-15.92	247.9	0.650	29.5	0.25
SkI5	0.156	-15.83	255.7	0.579	36.7	0.25
NL-I	0.151	-16.09	172.7	0.648	39.7	
NL-IT	0.151	-16.15	126.1	0.756	39.4	

Table 4:
Symmetric nuclear matter properties: ρ_{nm} is the equilibrium density, E/A the binding energy per particle, K the incompressibility, m^*/m the effective mass, a_4 the symmetry energy, and $\kappa_{sumrule}$ the sum rule enhancement factor. The effective nucleon mass given for the RMF parametrizations NL-Z, NL-I, and NL-IT is calculated at the Fermi surface i.e. at $k = k_F = 1.35fm^{-1}$. The values preceded by $\pm$ sign indicate the uncertainty of the prediction of the quantities obtained from the rules of error propagation in the fitting procedure. These uncertainties are the same for all the interactions in the same block, except for NL-IT.

the present uncertainty on this quantity. In fact, it turns out that K does not play an essential role for the question we discuss here. There are sizeable variations of the effective mass. The older force SkM* has the largest value. All the nonrelativistic fits performed in this work give lower effective masses. This is a consequence of the weight attributed to surface properties in the fitting procedure and also of the more systematic exploitation of all exchange parameters in the force. We note that the effective masses of the forces SKI3 and SkI5 are very small. This is the price paid for forcing a reproduction of the isotope shifts without having the full freedom in the spin-orbit force (b'_4 fixed). It casts some doubt on the quality of these interactions. It is interesting to note that the relativistic models NL-Z and NL-I have effective masses

at the Fermi surface which are comparable to those of the recent SHF paramerizations. The relativistic model with tensor couplings, NL-IT, behaves somewhat differently. Moreover, the uncertainties on nuclear matter properties associated with the fit NL-IT are rather large: $\Delta E/A = \pm 5.7$, $\Delta\rho_{nm} = \pm 0.06$, $\Delta K = \pm 104$, $\Delta m^*/m = \pm 0.1$, and $\Delta a_4 = \pm 15$. This indicates that this force has too many parameters so that the fitting procedure leads to a very shallow minimum in the χ^2 surface. For instance, the tensor fields can account separately for the spin-orbit splitting for a wide range of effective masses. In addition, the lowest χ^2 is reached for a very low incompressibility. This value comes however with a large uncertainty.

4.3 Results for finite nuclei and isotope shifts

The results obtained with the different relativistic and non relativistic parametrizations are summarized in the four parts of Fig. 4.3. They include three old parametrizations: the SHF force SkM* form [11], and the two RMF forces NL-Z from [12] and NL-SH from [38]. Each time, we have used the prescription for the centre-of-mass correction to the total energy $E_{c.m.}$ employed when the force was defined. For NL-Z and all the newly fitted forces, we have subtracted $E_{c.m.} = \langle \hat{P}^2_{c.m.} \rangle / 2mA$ after the solution of the Hartree-Fock equations.

In the second part of Fig. 4.3 we display results for the isotope shifts of *Ca*, *Sr* and *Pb*. The first column presents the experimental data. The second column shows the corresponding values corrected for the effects of GSC as discussed in the subsection (4.1). In our opinion, these are the values which should be compared to mean-field results. The corrections are small for *Pb* making this element a good test case. Although they are somewhat larger for *Ca* the corresponding error bars in both cases would not be bigger than the symbols we use in Fig. 4.3. As discussed above, the corrections are much larger for *Sr* and there is a discrepancy between the phenomenological estimate and the microscopic calculations within the generator coordinate method. In the figure, we have used the phenomenological estimate. We remind the reader that this large uncertainty on *Sr* isotope shift led us to exclude it from the fitted data.

We have seen that contrary to the two existing RMF sets NL-Z and NL-SH, the old Skyrme parametrization SkM* does not reproduce the isotope shifts in *Pb*. In fact, Fig. 4.3 is another representation of the result shown in Fig. 1. On the basis of just these old parametrizations one would be tempted to say that relativistic and non-relativistic models behave in a qualitatively different way with respect to isotope shifts. This holds not only for *Pb* but also for the isotope shifts of *Sr* and *Ca* as can

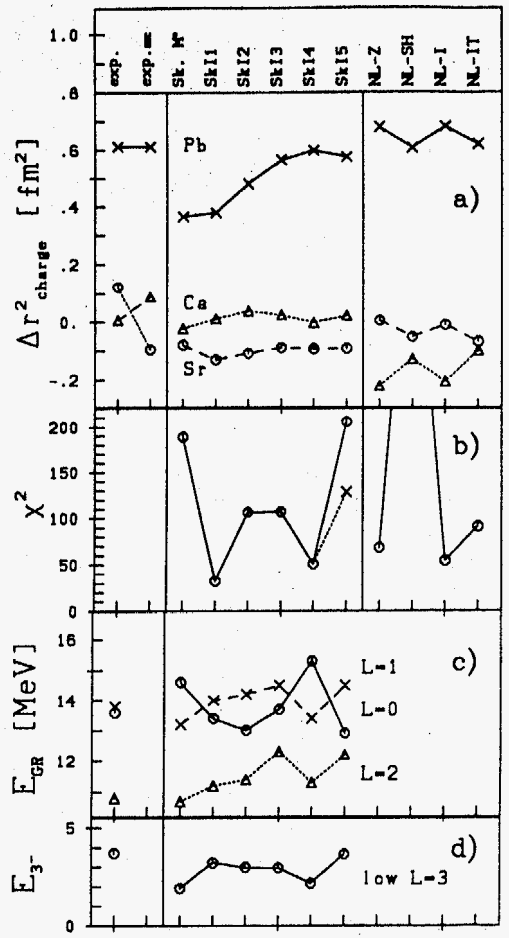

Figure 6:
Compilation of results for different parametrizations as indicated in the uppermost box. The box "a)" shows the isotope shifts on charge r.m.s. radii for ^{214}Pb-^{208}Pb, ^{84}Sr-^{88}Sr, and ^{48}Ca-^{40}Ca. The box "b)" shows the quality measure χ^2 where the dotted line excludes data on ^{16}O. In box "c)" follows the positions of the isovector L=1 resonance and the isoscalar L=0 and L=2 resonances in ^{208}Pb. The box "d)" shows the low lying 3$_-$ state in ^{40}Ca.

be seen from Fig. 4.3. The standard Skyrme forces fail for *Pb* while the RMF results disagree with *Ca* data. There are systematic differences for *Sr* but no conclusion can be drawn in view of the large uncertainty.

In part b) of Fig. 4.3, as an indicator of the overall agreement, we give the χ^2 over all data of Tab. 1 excluding the isotope shifts whose quality is displayed in part a). From the existing parametrizations, NL-Z looks the best. this is not too surprising since it has been designed according to the same procedure used here except for the exclusion of isotope shifts data. The χ^2 of the force SkM* is also remarkably low although this interaction was adjusted on fission barriers and surface tension, see [39], rather than on electromagnetic formactor as is done here. In view of the successes obtained with SkM* on many different properties like deformation or high spin properties, we think that it sets the order of magnitude for the value of χ^2 which can be considered acceptable. The χ^2 of NL-SH is close to 500. This large value reflects an agreement of lesser quality on surface properties. Indeed the adjustement of NL-SH concerning the features of nucleon distributions has been done on r.m.s. radii only. It would be interesting to check the predictions of this force for quantities very sensitive to surface properties such as the fission barriers. All newly fitted forces, of course, produce a χ^2 of fair quality.

The set SkI1 uses the standard Skyrme parametrization. However, contrary to SkM*, it exploits the degrees of freedom associated with the exchange parameters x_1, x_2 and x_3. Let us note here that the SkP force [40] designed to improve pairing matrix elements at the Fermi surface, also made use of these exchange parameters. The value of its χ^2 (≈ 200) compares well with that of SkM*. We have already mentioned that its predictions for isotope shifts are also similar to those of SkM* and of any other old Skyrme forces. The new fit SkI1 does not take into account the isotope shifts and leads to a much smaller χ^2 than that of the old Skyrme force. On the other hand, as expected, it underestimates the isotope shifts in *Pb* as the older SHF parametrizations. The predicted isotope shift for *Ca* is acceptable while that for *Sr* is slightly too small.

The set SkI2 results from a fit of the same standard SHF parametrization to all data of Tab. 1, including now the isotope shifts in *Ca* and *Pb*. At the cost of a factor three increase in the χ^2, one reduces by half the disagreement on *Pb* isotope shifts. The kink in the radius evolution at N=126 is still underestimated. The results on *Ca* and *Sr* isotope shift remain of the same quality.

In a next stage, we have analyzed the SHF model with the generalized spin-orbit energy (6) keeping the parameter b'_4 fixed at zero to simulate the density mix of the RMF. A fit to the data contained in Tab. 1 yields the set SkI3 which describes correctly

the isotope shift in *Pb*. On the other hand, the χ^2 is as large as that of SkI2. Again there is little change concerning the *Ca* and *Sr* shifts.

A fit to all data in which the constraint on b'_4 is relaxed, leads to the set SkI4. This set provides the best overall agreement on both, isotope shift and ground state properties. For the latter it performs almost as well as SkI1. In addition good agreement on *Pb* data is now achieved. This vindicates the discussion of Sect. 2 and shows the important role played by the spin-orbit component of the functional. From Tab. 3 one sees that b_4 and b'_4 have nearly opposite values. In view of Eq. (7), this implies that the *neutron* spin-orbit strength of SkI4 depends almost only on the *proton* density and vice versa. This is at variance both with the usual SHF model where the weights of neutron and proton densities are respectively two and one, and with the RMF model which predicts equal weights for both densities. In Figs. 2 we compare the single particle spectrum of SkI4 with that of conventional forces. With SkI4 one finds a large gap in the single-particle neutron spectrum which is similar to that found with the RMF model using the NL-Z parametrization. This confirms our presumption on the close relation between the gap in the neutron spectra and the kink in the charge radii isotope shifts. The height of the peak of the spin-orbit potential of SkI4 lies between that of NL-Z and SkM* (see Fig. 4). However, because the width of the peak is narrower than that of NL-Z, their integrated spin-orbit strengths are very close. This indicates that details of the radial dependence of W are not very crucial even for such a delicate nuclear property as the charge isotope shifts.

For the reasons discussed in subsection 4.1, we have performed a fit within the standard SHF model on a set of data including the isotope shift but omitting the binding energy, radius, and surface thickness of ^{16}O. Note that the spin-orbit splitting of this nucleus has been kept in the data set. The result is the set SkI5. This set manages to reproduce correctly the isotope shift in *Pb* within the conventional SHF model. The χ^2 of SkI5 is plotted in two ways: i) the χ^2 for the fitted data set (points joined by the dashed lines), ii) the χ^2 for the complete set including the ground state properties of ^{16}O (points joined by solid lines). The jump in χ^2 is dominated by the binding energy of ^{16}O which comes out 1.6% to high. This is a large discrepancy in view of the average error on the binding energy of 0.3%. Furthermore, as mentionned above, the effective mass of SkI5 may be too small (Tab. 4). On the other hand, SkI5 provides a counterexample to the conjecture that the standard SHF model is not able to reproduce the isotope shifts properties. We note that SkI5 achieves this result by a mechanism not related to the spin-orbit term. The neutron spectrum of SkI5 (Fig. 2) is similar to that of NL-Z and SkI4. On the other hand, the spin-orbit potential (Fig. 4)

resembles that of SkM*. This example shows that the intermediate step of our analysis is still valid. It is indeed the gap in the neutron spectra which explains the kink in the isotope shifts. However, the parametrization SkI5 produces the gap by means of its low effective mass which decreases the spectral density. Whether this mechanism has unwanted side effects has still to be explored. We have already noted the lower quality of the ^{16}O binding energy. Other observables, such as nucleon scattering, deformation properties and fission need yet to be investigated.

In section 2, our reasoning relating charge isotope shift to neutron spectrum implied that the kink observed in the evolution of charge radii was the consequence of the same behavior in the neutron radii. On the lower part of Fig. 1 we show that indeed the neutron radii curves of SkI4 and SkI5 exhibit a kink very much alike that of NL-Z. Finally the charge radii curves (upper part of the Fig. 1) show that the p-n attraction characteristics of all parametrizations must be very similar. Because they almost overlap the NL-Z, SkI4 and experimental curves we have not plotted the results for SkI5 in the upper part of Fig. 1.

The Fig. 4.3 continues with the RMF models. Already the existing relativistic parametrizations NL-Z and NL-SH gave good agreement for the isotope shift of *Pb*. The set NL-Z provides even already a low χ^2, although somewhat larger than for the best SHF sets here. The *Sr* isotopes look also more reasonable. But a new problem appears which was not much recognized up to now: the isotope shift in *Ca* is poorly reproduced. This has motivated us to refit the RMF model with the data on isotope shifts included where now the question is how much flexibility exists to accomodate the data on *Ca*. The result is the set *NL-I*. It is obvious that the isotope shifts did not move much. But they did not spoil the quality measure χ^2 either. (The slight improvement on χ^2 over NL-Z is due to minor differences in the data set used in the fit.) The model is simply ignoring that inconvenient piece of information.

In an attempt to remove this remaining weakness of the RMF model, we have investigated several possible extensions. Among them, we tried without success the addition of a δ meson (scalar-isovector) and the introduction of more involved nonlinearities as described in [41]. Exploring further the idea that spin-orbit properties could be responsible, we have investigated an extension by tensor coupling of the vector and of isovector-vector field because these have an immediate impact on the spin-orbit force, see [5, 12]. The resulting set is NL-IT, shown in the last column of Fig. 4.3. This indeed moves the isotope shifts in *Ca* towards the desired regime without spoiling the shifts in *Pb* and with an acceptable degradation of the overall quality. The example demonstrated that there is yet some unused space for development in the RMF. On

the other hand, we take the set NL-IT with some reservation. The Tab. 4 shows a unusually low incompressibility and the effective mass is rather large compared to all other RMF sets. The set seems to have also some intrinsic redundancy because the extrapolation errors, e.g. on nuclear matter properties, are one order of magnitude larger than with any other model.

Coming back to the isotope shifts results displayed in Fig. 4.3, we note that the SHF parametrizations behave similarly for *Ca* and *Sr* isotopes although their prediction can vary for *Pb*. Moreover they differ from the RMF results. In particular, the isotope shifts in *Ca* are poorly reproduced by the RMF models while SHF models give a much better agreement.

The part c) of Fig. 4.3 presents results on giant resonance modes in ^{208}Pb for the Skyrme functionals. The energies correspond to position of the dominant peak. They have been computed within the local RPA, as described in [14, 42]. The energies of the isoscalar monopole and quadrupole resonances are strongly constrained by the ground-state data which are more or less equally well described by the SHF models. Accordingly, we see little variation in the resonance properties and the energies agree well with data. For the isovector dipole resonance ($L = 1$), there is a somewhat large fluctuation among the forces. In fact, it would be much larger had we not enforced the value of the sum rule enhancement factor κ (eq. (12)) which sets a constraint on the the isovector properties of the force. It is gratifying to see that the value of $\kappa = 0.25$ supported by an analysis of different observables [31] provides fits with reasonable energies for the dipole giant resonance. For the five SHF parametrizations introduced in this work, the difference with the experimental dipole energy never exceeds 1.5MeV.

In the lower part of the Fig. 4.3, we have reported results for the energy of the low-lying octupole mode in ^{40}Ca. Depending on the force, this energy can vary by more than 2MeV. It is known that this mode is very sensitive to the spectral density at the Fermi energy. Comparing standard SHF forces (SkM*, SkI1, SkI2, and SkI5), one sees a correlation between the energy and the the effective nucleon mass given in Tab. 4. The influence of the effective mass can be compensated by the the spin-orbit force, as it is the case for the sets SkI3 and SkI4. This is another example of an observable which is significantly affected by the action of the effective mass and the spin-orbit term force on the single-particle spectrum density. The effective mass seems to have the stronger impact in case of *Ca* whereas the spin-orbit force plays a more important role in *Pb*. We note however that all calculated energies are below experiment. This may be an artefact of the zero-range nature of the Skyrme force which exaggerates the (attractive) effect of core polarization through coupling to extremely high energy

states [33].

Finally, we want to comment on the parameters of the Skyrme forces as given in Tab. 3. By an analysis of the normal and ferromagnetic phases of neutron matter it was shown in [43] that the range of acceptable values for the parameter x_2 is limited to the interval $[-1.25, -1]$. It is remarkable that all our fits conducted without taking into account this constraint leads to values compatible to or not far from this interval. It seems therefore that the additional criteron discussed in [43] could easily be introduced in a systematic determination of a Skyrme like functional.

5 Conclusions

In this work we have tried to determine the origin of the different behaviors of the relativistic and non-relativistic mean-field models concerning the isotope shifts of the charge radius at the shell closure $N = 126$. We first analyzed the results obtained with an existing parametrization of each model: the nonrelativistic Skyrme force SkM* often employed in nuclear structure calculations, and the relativistic NL-Z parametrization which has been tested to accurately reproduce the ground state properties of many spherical nuclei. We have found that, because of the strong p-n attraction, the evolution of the charge radius as a function of N was governed by that of the neutron distribution through self-consistency. Then we have shown that the contrasted behaviors of the two models for the neutron radii can be related to differences in neutron single particle spectra at the Fermi energy. The relativistic model produces a large gap at the Fermi energy of ^{208}Pb whereas the spectrum of SkM* is more dense. In a next step, we have argued that this behaviour was mostly due to the difference in the strength of the spin-orbit term in the single-particle Hamiltonian. The SkM* strength is about 30% larger than that of NL-Z. As a consequence, for the $1g_{9/2}$ orbital occupied in the heavier Pb isotopes, the SkM* functional predicts an energy which is more than 1MeV lower. The root mean square radius of this orbital is therefore smaller so that the growth of the neutron radius in SkM* versus N is slower. In turn, this explains why SkM* does not reproduce the observed rapid increase of the charge radius well described by the relativistic model.

We have then analyzed the differences between the spin-orbit properties of the relativistic and nonrelativistic model. As tool for the comparison, we have used a nonrelativistic reduction of the relativistic model. Among the structural differences of the spin-orbit contributions to the mean-field Hamiltonian, only one seems to be important: the two models do not use the same density dependence for the neutron

spin-orbit potential. For the Skyrme force, it depends on the sum $2\rho_n + \rho_p$ while it is a linear function of $\rho_n + \rho_p$ for the RMF. In order to investigate in more details the influence of the spin-orbit term, we have introduced a generalization of the Skyrme functional in which the relative weights of the neutron and proton contributions to the spin-orbit strength can be freely adjusted.

To explore the potentialities of both models we have determined new parametrizations by means of a fit on a set of data including ground state properties of spherical nuclei from ^{16}O to ^{208}Pb plus the isotope shift evolution for the Ca and Pb elements. It turns out that the best conventional Skyrme functional (SkI2) cannot account for the isotope shifts and at the same time produce a a low χ^2 on the nuclear ground-state properties included in our standard set of data. On the other hand, the generalized spin-orbit functional, allows a high quality agreement on the complete set of data (set SkI4). The optimal parametrization is such that the neutron spin-orbit form factor depends almost only on the proton density ρ_p. In any case, we come to the conclusion that an agreement on the isotope shifts in Pb is not proprietary to the relativistic models.

Somewhat surprising is the further observation that, with the standard Skyrme functional, one can also explain the isotope shifts if one accepts a lower quality reproduction of the binding energy ^{16}O (a 2.0MeV overbinding). The corresponding parametrization SkI5 uses a different mechanism to achieve its goal, namely a low effective mass. This example shows that the kink observed in the charge radius isotope shift of Pb can be described accurately with the standard Skyrme functional. However, it remains to assess whether in addition to the inaccurate ^{16}O binding energy the set SkI5 does not suffer from other weaknesses caused by its small effective masses.

The relativistic models have difficulties to explain the isotope shifts in Ca which on the other hand are generally well reproduced by the Skyrme functionals. A first attempt to cure that problem explored a generalized relativistic functional which includes tensor coupling. The generalized model was indeed able to improve the case of Ca in the right direction. But the model then introduces some other features which require further exploration before this point can be considered to be settled.

We are thus led to change our appraisal of the potentialities of both models. As we began this analysis, it seemed that the relativistic model was performing better than the Skyrme functional with respect to the isotope shifts in Pb. We have cured this apparent deficiency of the non relativistic description by a minimal extension of the Skyrme functional. On the other hand, our results seem to indicate that the relativistic model has difficulties explaining Ca isotope shift. We are still exploring this question.

In conclusion let us note that in our opinion, the scope of the present analysis which relies mostly on nuclei in the vicinity of the stability line is too limited to permit us to make a definitive choice between the several density dependences of the neutron spin-orbit potential: $\propto 2\rho_n + \rho_p$ for the Skyrme force, $\propto \rho_n + \rho_p$ for the RMF model, or $\propto \rho_p$ for the generalized functional SkI4. In view of these widely different weights on neutron and proton densities, a more complete investigation with an enlarged set of data including exotic nuclei appears necessary if one wants to predict accurately the evolution of single particle spectra and therefore the shell effects in the vicinity of the drip lines.

References

[1] D. Vautherin, D.M. Brink, Phys.Rev. **C5** (1972) 626

[2] P. Quentin, H. Flocard, Ann.Rev.Nucl.Sci. **28** (1978) 523

[3] J.D. Walecka, Ann.Phys. (N.Y.) **83** (1974) 491

[4] B.D. Serot, J.D. Walecka, Adv.Nucl.Phys. **16** (1986) 1

[5] P.-G. Reinhard, Rep.Prog.Phys. **52** (1989) 439

[6] V. Blum, J.A. Maruhn, P.-G. Reinhard, W.Greiner, Phys.Lett. **B323** (1994) 262

[7] N. Tajima, P. Bonche, H. Flocard, P.-H. Heenen, M.S. Weiss, Nucl.Phys. **A551** (1993) 434

[8] M.M. Sharma, M.A. Nagarajan, P. Ring, Phys.Lett. **B312** (1993) 209

[9] S.A. Fayans, S.V. Tolokonnikov, E.L. Trykow, D. Zawischa, Phys.Lett. **B** (1994)

[10] J. Dobaczewski, W. Nazarewicz, Phys.Rev.Lett. **73** (1994) 1869

[11] J. Bartel, P. Quentin, M. Brack, C. Guet and H.-B. Hakansson, Nucl. Phys. **A386** (1982) 79.

[12] M. Rufa, P.-G. Reinhard, J.A. Maruhn, W. Greiner, M.R. Strayer, Phys. Rev. **C38** (1989) 390

[13] M. Rufa, J.A. Maruhn, W. Greiner, P.-G. Reinhard, J. Friedrich, Z. Phys. **A323** (1986) 323

[14] P.-G. Reinhard, Ann.Phys. (Leipzig) **1** (1992) 632

[15] S. Weisgerber, P.-G. Reinhard, Ann.Phys. (Leipzig) **2** (1992) 666

[16] M. Beiner, R.J. Lombard, Ann.Phys. (N.Y.) **86** (1974) 262

[17] Y.M. Engel, D.M. Brink, K. Goeke, S.J. Krieger, D. Vautherin, Nucl.Phys. **A249** (1975) 215

[18] J. Friedrich, P.-G. Reinhard, Phys.Rev. **C33** (1986) 355

[19] J.K. Tuli, *Nuclear Wallet Cards*, National Nuclear Data Center, Brookhaven National Laboratory, Upton 1985

[20] J. Friedrich, N. Voegler, Nucl.Phys. **A373** (1982) 191

[21] E.B. Shera, E.T. Ritter, R.B. Perkins, G.A. Rinker, L.K. Wagner, H.D. Wohlfahrt, G. Fricke, R.M. Steffen, Phys.Rev. **C14** (1976) 731

[22] S.B. Dutter et al, Z.Phys. **A341** (1991) 39

[23] G.G. Simon, Ch. Schmitt, F. Borkowski, V.H. Walther, Nucl.Phys. **A333** (1980) 381

[24] G.G. Simon, Ch. Schmitt, V.H. Walther, Nucl.Phys. **A364** (1981) 285

[25] P.-G. Reinhard , D. Drechsel, Z. Phys. **A290** (1979) 85

[26] F. Barranco, R.A. Broglia, Phys.Lett. **B151** (1985) 90

[27] F. Buchinger et al, Phys.Rev. **C41** (1990) 2883, and references cited therein

[28] P. Bonche, H. Flocard, P.H. Heenen, S.J. Krieger, M.S. Weiss, Nucl.Phys. **A443** (1985) 39

[29] J.P. Blaizot, Phys.Rep. **64** (1970) 171

[30] J.M. Eisenberg, W. Greiner, *Nuclear Theory 2: Excitation Mechanism of the Nucleus*, North-Holland, Amsterdam 1970

[31] E. Chabanat, P. Bonche, P. Haensel, J. Meyer, F. Schaeffer, Proceedings of the conference SELMA 1994, to appear in Physica Scripta Suppl.
E. Chabanat, P. Bonche, P. Haensel, J. Meyer, F. Schaeffer, preprint 1994

[32] P.-G. Reinhard, Phys.Lett. **A169** (1992) 281

[33] F. Barranco, P.F. Bortignon, R. Broglia, P.-G. Reinhard, in preparation

[34] M. Girod, P.-G. Reinhard, Nucl.Phys. **A384** (1982) 179

[35] P.-H. Heenen, P. Bonche, J. Dobaczewski, H. Flocard, Nucl.Phys. **A561** (1993) 367

[36] S. Raman, C.H. Malarkey, W.T. Miltner, C.W. Nestor, P.H. Stelson, Atomic Data and Nuclear Data Tables **36** (1987) 1

[37] K.W. Schmid, P.-G. Reinhard, Nucl.Phys. **A350** (1992) 283

[38] M.M. Sharma and P. Ring, Phys. Rev. **C45** (1992) 2514.

[39] M. Brack, C. Guet, H.-B. Hakansson, Phys.Rep. **123** (1985) 275

[40] J. Dobaczewskki, H. Flocard, J. Treiner, Nucl.Phys. **A422** (1984) 103

[41] C. Greiner, P.-G. Reinhard, Z.Phys. **A342** (1992) 379

[42] Y. Gambhir, P.-G. Reinhard, Ann.Phys. (Leipzig) **1** (1992) 598

[43] M. Kutschera, W. Wójcik, to appear in Phys.Lett. **B** (1994)